^{2}H$(d,\gamma)^4$He polarization observables at 20, 30, and 50 MeV

R. M. Whitton* and H. R. Weller
Triangle Universities Nuclear Laboratory and Duke University, Durham, North Carolina 27706

E. Hayward† and W. R. Dodge‡
National Institute of Science and Technology, Gaithersburg, Maryland 20899

S. E. Kuhn§
Lawrence Berkeley Laboratory, Berkeley, California 94720
(Received 2 June 1993)

Tensor and vector analyzing powers for the ^{2}H$(d,\gamma)^4$He reaction have been obtained as a function of angle at E_d(lab) = 20, 30, and 50 MeV. Differential cross sections were extracted at 30 and 50 MeV. Data for $A_{yy}(\theta)$ and $A_y(\theta)$ were obtained at all three energies, while $T_{20}(\theta)$ was also measured at E_d(lab) = 50 MeV. A direct capture calculation was performed and compared to the data. This calculation assumes point deuterons and that the reaction proceeds primarily via $E2$ radiation in this energy region. A value of 4% for the D-state probability arising from two-deuteron relative motion in the ^{4}He wave function was extracted by fitting the predictions of this model to the data. This calculation indicates that g-wave capture is significant at the energies of the present experiment, a result which is supported by a transition matrix element analysis of the data. The results of a microscopic 7-channel resonating group model (MCRGM) calculation are also compared to the data. This model takes all amplitudes having incoming angular momenta $l \leq 2$ into account as well as the couplings to the n-^{3}He and p-T channels. This microscopic calculation, which has produced reasonable agreement with the previous low energy data, predicts a value of 2.2% for the two-deuteron component of the D state in ^{4}He. There is qualitative agreement with the present data.

PACS number(s): 25.40.Lw, 25.10.+s, 24.70.+s

I. INTRODUCTION

The D-state probability in ^{4}He has been a subject of intense study in recent years. A recent review covers both the theoretical predictions and the experimental results [1]. If a conclusion can be drawn from recent theoretical efforts, it is that calculations of the D-state probability are highly sensitive to the model and computational method used. A wide range of results has been obtained, even with the same potentials. For example, Goldhammer [2] obtains 5.36% while Meder *et al.* [3] get 14.2% for the total ^{4}He D-state probability, both using the Paris potential and being in essential agreement on the binding energy. The most recent calculation uses the Green's function Monte Carlo method and a range of two-body potentials. The results of this study [4] indicate a total D-state probability in ^{4}He of around 17%.

Radiative capture experiments have provided some of the best evidence for the presence of D states in light nuclei, but a model must be used to interpret the results in terms of an absolute probability. Since they arise from interference effects, polarization observables can provide a sensitive probe of small admixtures of transition amplitudes related to small components in the ^{4}He wave function. Analyzing powers on the order of 30% are reported in this work. They are thus a powerful tool for studying some of the more subtle aspects of the ^{4}He nucleus and the dynamics of the ^{2}H$(d,\gamma)^4$He reaction.

Vector (A_y) and tensor (A_{yy}) analyzing powers have been measured as a function of angle (θ) at beam energies of 20, 30, and 50 MeV. The differential cross section (σ) has been measured as a function of angle at beam energies of 30 and 50 MeV. The tensor analyzing power [$T_{20}(\theta)$] was also measured at 50 MeV. These data augment an extensive set of data obtained at TUNL [5,6] and Wisconsin [7–9] at E_d(lab) $\leq$ 15 MeV, as well as from a recent measurement of the differential cross section at 30 MeV [10] and a measurement from IUCF at E_d(lab) = 95 MeV [11]. The present measurements show that $A_{yy}(\theta)$ remains fairly isotropic but peaks in magnitude near E_d(lab) = 30 MeV.

Within the pure $E2$ approximation a tensor analyzing power can only arise from a tensor-force effect in this reaction. The large observed values of the tensor analyzing powers obtained in this study will be shown to suggest that a significant fraction of the capture cross section arises as a result of the presence of a D state in the ground state of ^{4}He. Below 15 MeV significant

*Present address: 1107 Seminole Drive, Tallahassee, FL 32301.
†Present address: 8400 Westmont Court, Bethesda, MD 20817.
‡Present address: George Washington University, Washington, D.C. 20052.
§Present address: Old Dominion University, Norfolk, VA 23529.

p-wave capture strength complicates the analysis of this reaction, while at 95 MeV the long wavelength approximation and the neglect of higher multipoles may be invalid. The best determination of the D state in ^{4}He may therefore be possible in the previously unprobed energy region of 20–50 MeV.

In 1950 Flowers and Mandl [12] pointed out that to the extent that the electric and the magnetic operators depend respectively only on the spatial and spin coordinates of the nucleon, the $^2\mathrm{H}(d,\gamma)^4\mathrm{He}$ reaction should be dominated by isoscalar $E2$ radiation. It can be seen that, because the incident deuterons are identical bosons, only scattering states with $L+S$ even are allowed. This forbids $\Delta S = 0$ $E1$ transitions since $L = 1$ is required in the incident channel to form a 1^- state so that S must equal 1, while the ground state has $L = 0, S = 0$ with a small $L = 2, S = 2$ admixture. The only possible $E1$ amplitudes are thus the $\langle {}^1S_0 \mid E1 \mid {}^3p_1\rangle$ and $\langle {}^5D_0 \mid E1 \mid {}^3p_1\rangle$ transition matrix elements (labeled as a $\langle {}^4$He component|multipolarity| initial scattering state$\rangle$ and with notation $^{2S+1}L_J$). These are zero for the normal spin-independent part of the $E1$ operator in a two-point-deuteron capture model. In addition, $E1$ is inhibited in the $^2\mathrm{H}(d,\gamma)^4\mathrm{He}$ reaction by the isospin selection rule for self-conjugate nuclei ($\Delta T = 1$) [13]. As will be discussed below, coupled-channel effects, the spin-dependent part of the $E1$ operator, and tensor-force effects can generate finite $E1$ radiation.

The contribution of the magnetic part of the electromagnetic operator is reduced by a factor of $\hbar\sqrt{10}/(McR) \approx 0.15$ compared to the electric part, where M is the projectile mass, and R is the radius of the nucleus [14]. In the present reaction, there is only one possible $M1$ capture amplitude, the $\langle {}^5D_0 \mid M1 \mid {}^5 d_1\rangle$ which is a transition to the (small) D-state component of the ^{4}He ground state. The isospin selection rule should also give a considerable inhibition of this $\Delta T = 0$ transition [13]; $M1$ strength is thus expected to be small.

There are three possible $M2$ amplitudes but, as noted in earlier work [15,1], they would manifest themselves as an odd order Legendre function (and hence an asymmetry about 90°) in the tensor analyzing powers as a result of interference with the dominant $E2$ terms. There are no large asymmetries and thus little convincing evidence for the presence of $M2$ strength in the present data. Mellema *et al.* have taken a complete data set at 2.5 MeV, and their multipole decomposition supports the presence of $M2$ radiation at this energy [7].

$E2$ radiation with $\Delta S = 0$ is allowed from a 2^+ continuum state formed via $l = 2$, $s = 0$ going to the $^1S_0$ ground state and by states formed with $l = 0$, 2, or 4 and $s = 2$ going to the $^5D_0$ component (D state) of the ^{4}He ground state. As $S = 0$ and $S = 2$ can triangulate with 2, an interference of the predominant d-wave capture to the large S-state part of the ^{4}He ground state, with s-, d-, or g-wave capture leading to the small D-state part, is expected to be the dominant source of finite tensor analyzing powers.

The preceding arguments imply that this reaction is predominantly $E2$ and that within this approximation a tensor analyzing power can arise mainly as a result of the presence of transitions going to the D state in ^{4}He.

The vector analyzing power $A_y(\theta)$, arises primarily as a result of interference of the predominant $E2$ radiation with other multipoles, probably $E1$ and/or $M2$, especially at the lower (< 15 MeV) energies. While A_y is rather large at very low energies [6], our measurements show that it becomes small at around 15 MeV and remains fairly consistent with zero up to 50 MeV. The origin of the non-$E2$ radiation apparent at lower energies has been the subject of some discussion. It has been conjectured that the charge polarization of the deuterons could break the conservation of isospin and thus may be the mechanism that produces $E1$ transitions.

To investigate this notion, suppose we define a set of internal coordinates for the ^{4}He nucleus, as in Fig. 1, where $\mathbf{r}$ and $\mathbf{r}'$ are the internal coordinates of the deuterons, $\boldsymbol{\rho}$ is the position of one of the charges with respect to the other one, and $\mathbf{s}$ is a vector between the centers of mass of the deuterons. The potential energy due to the Coulomb force is, in rationalized units, simply the proton charge squared divided by the distance between them:

$$V_c = \frac{e^2}{\rho} = \frac{e^2}{\sqrt{s^2 + \frac{1}{4} \mid \mathbf{r} - \mathbf{r}' \mid^2 + \mathbf{s}\cdot(\mathbf{r} - \mathbf{r}')}}. \qquad (1)$$

A potential which retains the internal coordinates of the deuterons can be expressed, using the binomial theorem, in the form

$$V_c = \frac{e^2}{\rho} = \frac{e^2}{s} - \frac{e^2}{2s^2}\,\hat{s}\cdot(\mathbf{r} - \mathbf{r}') + \cdots, \qquad (2)$$

for $s \gg |\mathbf{r} - \mathbf{r}'|$. The second term can be viewed as a polarization potential and applied as a perturbation to the point deuteron Hamiltonian (the first term). To first and second order, all corrections vanish because the operands are even for this case of identical bosons, while this operator is odd. The next higher order in the binomial expansion produces terms which are quadrupole in nature and thus cannot be the source of $E1$ transitions. It is concluded that charge polarization is not a source of $E1$ radiation in this reaction [16].

$E1$ can, however, come about through the isoscalar spin-dependent part of the $E1$ operator. This part of the $E1$ operator has often been ignored in previous studies but is important in this reaction because the normally dominant isovector (non-spin-flip) $E1$ is forbidden by the aforementioned symmetry and isospin considerations.

The tensor analyzing powers $A_{yy}(\theta)$ and $T_{20}(\theta)$ were

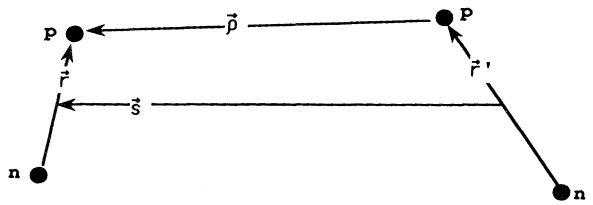

FIG. 1. Internal coordinates of the ^{4}He nucleus which include the internal coordinates of the deuterons.

measured at 50 MeV. Since s-wave capture to the D state of ^{4}He contributes to first order in T_{20}, but only to second order in A_{yy}, both observables are important in a transition-matrix element analysis. T_{20}, however, does not lend itself as well to the simple interpretations that have been outlined as does A_{yy}. This is because the D state of the deuteron plays a stronger role in the s-wave capture which contributes to T_{20}. An $l = 0$ (s-wave) scattering state can couple via $E2$ to the large $L = 0$ part of the ^{4}He ground state via an internal $\Delta L = 2$ transition in a deuteron. This could be a transition from the deuteron D to S state, S to D state, or D to D state. An $l = 2$ (d-wave) scattering state can couple to the D-state component of ^{4}He in this same way but, since the D state is small, this is not expected to be important. There is not enough internal angular momentum to couple an $l = 4$ (g-wave) scattering state to the $L = 0$ ground state in this way.

An additional source of difficulty in describing T_{20} could be the fact that the s-wave scattering state is highly distorted and therefore difficult to describe with this model.

II. EXPERIMENTAL DETAILS

There were a number of major difficulties that had to be overcome in order to accomplish these measurements successfully. The cross section for the reaction studied in this work is very small ($\simeq$ 10 nb/sr), while other ^2H+d induced reactions produce an intense background of energetic and thermal neutrons. There is also a neutron and gamma-ray background associated with the target windows. As the energy is increased, the advantage of the high Q value (23.8 MeV) of the capture reaction is lost and the Coulomb barrier in heavy materials is overcome.

The unpolarized differential cross section at E_d(lab) = 30 MeV was obtained at the variable energy AVF cyclotron of the Kernfysisch Versneller Instituut (KVI) in Groningen, The Netherlands. The remainder of the data were obtained at the 88-Inch Cyclotron of the Lawrence Berkeley Laboratory (LBL). All measurements were made using large anticoincidence-shielded NaI gamma-ray spectrometers. The measurements at 50 MeV required the detection of the recoiling ^{4}He nuclei in coincidence with the gamma rays along with time-of-flight (TOF) criteria for clean event identification.

The data at 20 MeV were the first taken at LBL and were obtained using a deuterated polyethylene foil as the target. The thickness of deuterium was about 5 mg/cm^2, but tended to change as the foil was burned away by the beam, thus requiring careful monitoring. These data suffer from poor statistics, providing a motivation for building thicker gas cell targets for all subsequent work. The gas was contained within the cells by 0.0254 mm Kapton windows, the total D_2 thickness being 45 mg/cm^2. The KVI target, used to measure the unpolarized differential cross section at 30 MeV, was a cylindrical gas cell 7.6 cm in diameter with 1.9 cm diameter Kapton windows for the beam to enter and exit. In order to maximize the ratio of target deuterium to foil window thickness the cell was kept at liquid nitrogen temperature. This scheme improves the ratio by a factor of around 3. In addition to the beam windows there was a small window at 30° to the beam axis through which a solid state detector viewed a small region of the interior of the target cell. This window was 0.16 cm wide and 1.9 cm tall, and was also covered by Kapton. In this geometry the detector viewed a region within the target through which all the beam had to pass. The angle from which this monitor detector viewed the target was thereby made independent of the exact position of the beam. This cell was pressurized to an absolute pressure of 404 kPa.

The remainder of these data were taken at the 88-Inch Cyclotron at the Lawrence Berkeley Laboratroy (LBL). The LBL target assembly was similar to the KVI target though 10.16 cm in diameter and without the monitor. This cell had a 3.8 cm exit window designed to allow the recoiling ^{4}He nuclei to escape the target to be detected in coincidence with the gamma rays. This target was typically filled to 303 kPa for a thickness similar to the KVI target.

The NaI spectrometer systems included active and passive shielding, gain stabilization, and antipileup circuitry. Three different, but very similar NaI spectrometers [17] were used in taking these data: one at KVI and two at Berkeley (two more were used extensively at TUNL in preparation and testing). All three NaI crystals were 25.4 cm in diameter. The two used at LBL were 25.4 cm deep while the KVI spectrometer was 30.5 cm deep. Anticoincidence shields of fast plastic scintillator surrounded the NaI crystals and typically could be used to reject around 99% of the events produced by cosmic radiation passing through the NaI crystals and shields. Each assembly was surrounded by lead shielding 7.62–12.7-cm thick. Outside of the lead was 20–50 cm of neutron shielding consisting of boric acid, ^{6}Li hydride, lithium carbonate, concrete, and water in various configurations depending on the run. While these spectrometers have a high intrinsic efficiency for the gamma rays that were produced in the capture reaction, the anticoincidence requirement also rejected a large fraction of the gamma-ray events due to escaping radiation being detected in the shield. While this phenomenon sharpened the resolution of the system by discarding events corresponding to gamma rays that did not deposit all their energy in the crystal, it reduced the efficiency and introduced uncertainty in measuring absolute yields. Attenuation of gamma rays by shielding material in front of the detectors also reduced the detector efficiency by about 30%. It should be noted that this affected the analyzing power measurements only through the reduction of the counting statistics. The runs at 50 MeV required the recoiling ^{4}He nuclei to be detected in coincidence with the capture gammas and this condition effectively eliminated the need for the shield anticoincidence requirement, allowing an increase of about 20% in counting statistics. All three NaI crystals were 25.4 cm in diameter. The two used at LBL were 25.4 cm deep while the KVI spectrometer was 30.5 cm deep. The spectrometers were actively stabilized against the gain shifts that could be caused by variations in the count rates in the photomultiplier tubes. Light

pulses produced in light emitting diodes optically coupled directly to the crystals were used as the reference.

The alpha recoil detection system used to identify capture events at E_d(lab) = 50 MeV took advantage of the fact that the recoiling ^{4}He nuclei are kinematically coupled in angle to the angle of the outgoing gamma ray and are restricted to a narrow forward cone in the region of $\theta < 7°$ from the direction of the beam. Unfortunately there was an intense background of deuterons elastically scattered from the beam on the target in this region. A count rate on the order of 10 MHz was expected in the recoil detectors due to the scattered beam. Figure 2 depicts the system which was constructed to enable the separation of the alpha particles of interest from the beam bursts by time of flight. A flight path of 2 m was chosen to allow a $\simeq$ 20 ns difference between the arrival times of the scattered deuterons and the alphas. This path length was sufficient to allow the recoiling alphas to be resolved from the beam bursts. Four identical detectors were employed, two on each side of the beam. The detectors were thin planes of fast plastic scintillator (Bicron BC418, 11.43 cm × 7.0 cm × 0.0762 cm) viewed by Hamamatsu R329 photomultiplier tubes through Lucite light pipes. The thickness was chosen so that the alpha particles of interest stopped in the first plane. The second plane was used to provide a fast veto to reduce the rate in some of the slower components of the electronics; when a deuteron was detected in the rear plane the pulse was vetoed in the very early part of the circuit while the time-to-pulse height converters and slow amplifiers remained ready to process the signal from an alpha particle that might arrive $\simeq$ 20 ns later. The recoil detector assemblies could be moved towards and away from the beam axis in order to optimize their position for a given gamma-ray detector angle.

Capture events of interest take place at all points within the target through which the beam passes. When the recoiling ^{4}He nuclei are produced, their momentum and energy are uniquely related to that of the gamma ray. For this reason it is possible to detect the two reaction products in coincidence with high efficiency. Unfortunately, once created, the recoiling nuclei are subjected to scattering from the other atoms in the target. The amount of energy loss and multiple scattering which a given nucleus experiences depends on the point in the target where it is created. The particles that are slowed the most come from the front part of the target where they have the greatest distance to travel to the detection plane. These effects combine to cause a skewed rectangular shape for the response in the TOF spectrum. The TOF spectrum was simulated using a Monte Carlo procedure which reproduced the shape of the recoil spectrum. The width of the time-of-flight peak was the limiting factor in choosing the target thickness.

Figure 3 shows a gamma-ray spectrum taken at 50 MeV with the various conditions placed on it to remove the background. It can be seen that the detection of the recoiling ^{4}He nuclei proved to be effective in producing a cleanly separated radiative capture peak.

It was desirable to minimize the area of the recoil detectors in order to minimize the counting rate produced by the scattered deuterons. The overall dimensions were chosen to catch all the alpha particles for the configuration of the gamma-ray detector that would produce the largest locus of recoils at the detection plane, with an additional margin included to accommodate the combined effects of multiple scattering and a beam divergence of 0.25°. A Monte Carlo simulation was carried out to understand these effects better. The Monte Carlo simulations proved to be important both in positioning the detectors for the highest efficiency and for estimating the efficiency as a correction to the yields as a function of angle. This correction cancels out in the determination of the analyzing powers.

The polarized deuteron beam at the 88-Inch Cyclotron was produced using an atomic beam [18] polarized ion

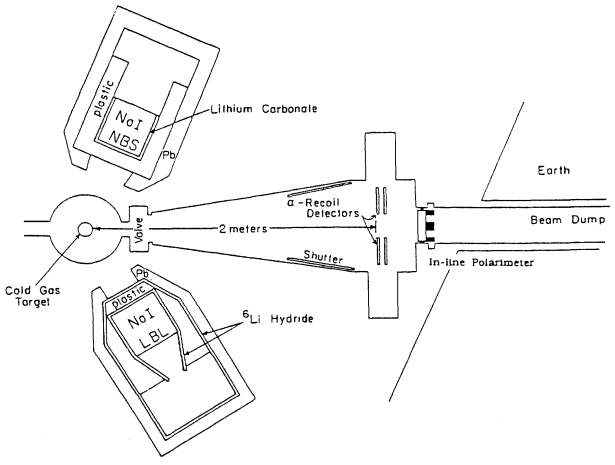

FIG. 2. The layout of the setup at LBL.

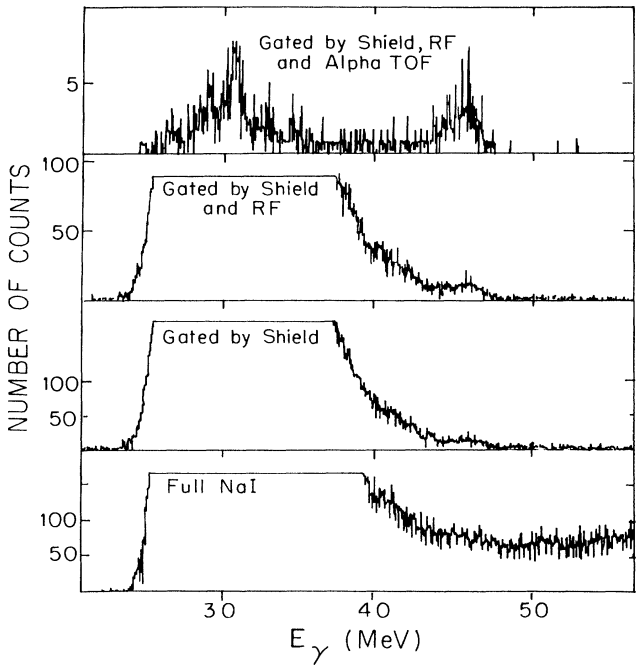

FIG. 3. Spectra taken at 50 MeV, with various cuts.

source [19]. Beam intensities of up to 70 nA with polarizations of 70–80 % of their maximum possible values ($\pm\frac{1}{3}$ for p_y and ±1 for p_{yy}) were typically available at the target. The various radio-frequency transition regions which produced states having different values of p_y and p_{yy} were switched on and off in equal intervals of roughly 1 sec and the data were routed appropriately. In this way, long term drifts in polarization or detector performance were unimportant.

Two polarimeters were used in this work. They were both in the target cave, requiring minimal retuning of the beam between measuring the polarization and taking data. The primary polarimeter consisted of a ^{4}He gas cell with Havar windows viewed by two $E-\Delta E$ type charged-particle telescopes. The telescopes were free to rotate to angles where previous measurements of the analyzing power were available. The thickness of the detectors was chosen such that most reaction products did not pass through the first plane. A slow coincidence requirement between the two planes of a telescope was all that was needed to identify the elastically scattered deuterons from the ^{4}He$(d,d)^4$He reaction. The polarization was measured every 8–12 h with this device.

We ran with three or four known and different combinations of weak and strong field transitions producing independent beam polarizations p_y and p_{yy}, typically $p_y = \pm0.25$ and $p_{yy} = \pm0.7$ for each case. With the polarization axis in the direction of the y axis, the cross section is expressed in terms of polarizations as

$$\sigma^i = \sigma_u(\theta,\phi)[1 + 3/2p_y^i A_y(\theta) + 1/2p_{yy}^i A_{yy}(\theta)],$$

$$i = 1-4, \tag{3}$$

where σ_u is the unpolarized cross section. Three or four equations must be solved, depending on the specific setup, for the three unknowns: σ, A_y, and A_{yy}. These are solved using a multilinear regression [20] fit, taking statistical errors in count rates and polarizations into account.

The measurement of T_{20} required that the spin axis not be perpendicular to the scattering plane (parallel to the direction of the magnetic field of the cyclotron) as it is when measuring A_{yy}. A large solenoid was installed in the capture beam line for the purpose of precessing the spin axis about the beam axis in order to measure T_{20}. This device consisted of a coil with 1096 turns and was 2.36 m long. It was driven with a current of 1000 A in order to generate an internal field of 5.5 kG and an integrated field of 13.1 kG m. When the spin precession solenoid was installed, the second polarimeter was built and installed in the beam dump just downstream of the recoil particle detectors. The target for this polarimeter was a carbon foil that was left in the beam at all times. It was viewed by four charged-particle detectors in two perpendicular scattering planes to confirm the calculated precession angle. The magnitude of the polarization was always measured in the ^{4}He polarimeter as well. The special beam dump polarimeter was needed only to verify the angle of precession, and the measured and calculated values for this were in agreement.

A. Error in analyzing powers

Because of the nature of the atomic beam type polarized ion source, there was little systematic error associated with the polarization of the beam. The changes between polarization states occur at a point where the beam is neutral in charge, and thus the steering is unaffected by any changes in the homogeneous magnetic field associated with the transition regions. Slow fluctuations in the beam position and current are averaged over all states by a fast (1 sec) spin flip, as are effects of changing target thickness and detector efficiency. For these reasons the systematic errors associated with the analyzing power measurements are diminishingly small compared to statistical errors associated with the polarimetry and the gamma-ray statistics. Propagation of these statistical uncertainties as well as the uncertainty in the analyzing power of the polarimeter are handled within the multilinear regression program used to calculate the observables [20]. The other possible source of error in the analyzing powers is associated with the finite geometry of the target and the detectors. There was not sufficient angular structure in the observables to make this a significant effect. The errors associated with a Monte Carlo correction procedure would have been on the order of the errors due to finite geometry, and so such a procedure was not applied. The errors quoted on all analyzing powers therefore arise purely from counting statistics and the uncertainty in the beam polarization.

B. Error in differential cross section

The angular distributions of the cross-section data contain systematic errors not present in the polarization observables. Possible sources of systematic error in the 50 MeV measurements include the beam integration, recoil detection efficiency, accidental ^{4}He vetoes, and electronics dead time. The sources of systematic error in the 30 MeV (singles) experiment included a difficult to determine background and accidental gamma-ray rejection owing to the anticoincidence shield. Finite geometry effects enter the measurements due to the angular structure of the cross section.

It was not possible to extract an absolute cross section. Only the corrected angular dependence of the differential cross section is presented.

Some background had to be subtracted from the sums at 30 MeV, as shown in Fig. 4. This background was estimated by interpolating between the backgrounds on both sides of the gamma-ray peak. This procedure makes a very small contribution to the quoted errors. Beam integration error was assumed to be constant with angle and is not included in the quoted errors at 50 MeV. The counting statistics in the beam monitor at 30 MeV produced an insignificant error.

Electronic dead times were compensated for by the use of a monitor at 30 MeV, and were measured to be less than 1% in the 50 MeV experiment. Accidental rejections due to the active shield were measured to be less than 10% at all times in the 30 MeV measurement.

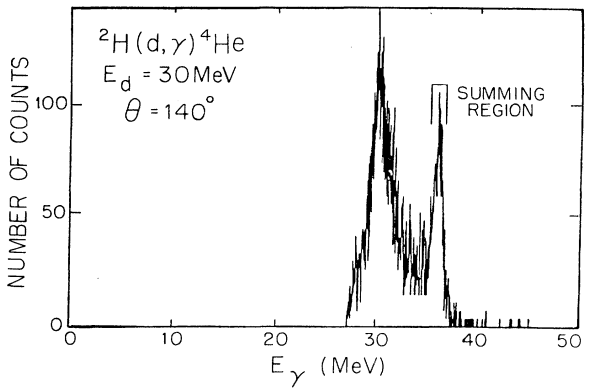

FIG. 4. Sample spectrum from the runs at 30 MeV.

The accidental rejection rate is believed to be known to within 20%, and so contributes an error of $< 2\%$ added in quadrature to the other sources of error. The anticoincidence shield requirement was not used in sorting the 50 MeV events, and so that measurement is free from this effect.

A large source of systematic uncertainty in the cross-section measurements at both 30 and 50 MeV is due to the large finite geometry of the apparatus and the rapid change with angle in the physical observables. A Monte Carlo procedure was used to correct these data for finite geometry effects. These corrections depend on an accurate guess of the physical cross section as a starting point, which is then averaged over the finite geometry of the target and the detector using a Monte Carlo procedure and compared to the measured values. When a consistent solution is reached, the guessed cross section is taken to be the finite geometry corrected data. The error in this procedure was estimated to be 10%.

The 50 MeV data can be affected by the loss of coincidence efficiency associated with alpha particles missing the scintillators. A Monte Carlo procedure was used to estimate the effects of the placement of the particle detectors, the multiple scattering in the target, and the beam divergence. While the placement of the detectors and the target thickness were known, the position and divergence of the beam were not so well known and were a large source of uncertainty. Accidental recoil vetoes associated with a scattered deuteron signal not having cleared in the second paddle is another source of systematic uncertainty. Because of these effects, the error in the differential cross section at 50 MeV is estimated to be 10% of the average cross section.

III. T-MATRIX ELEMENT ANALYSIS

The observables of this experiment can, following Ref. [21], be expanded in terms of Legendre and associated Legendre polynomials:

$$\sigma_u(\theta) = \sum_k A_k P_k(\cos\theta),$$

$$\sigma_u(\theta) A_y(\theta) = \frac{2}{3} \sum_k B_k P_k^1(\cos\theta),$$

$$\sigma(\theta) T_{20}(\theta) = \sum_k C_k P_k(\cos\theta),$$

$$\sigma(\theta) T_{22}(\theta) = \frac{1}{2} \sum_k E_k P_k^2(\cos\theta).$$

Since

$$A_{yy}(\theta) = -\frac{1}{\sqrt{2}} T_{20}(\theta) - \sqrt{3}\, T_{22}(\theta),$$

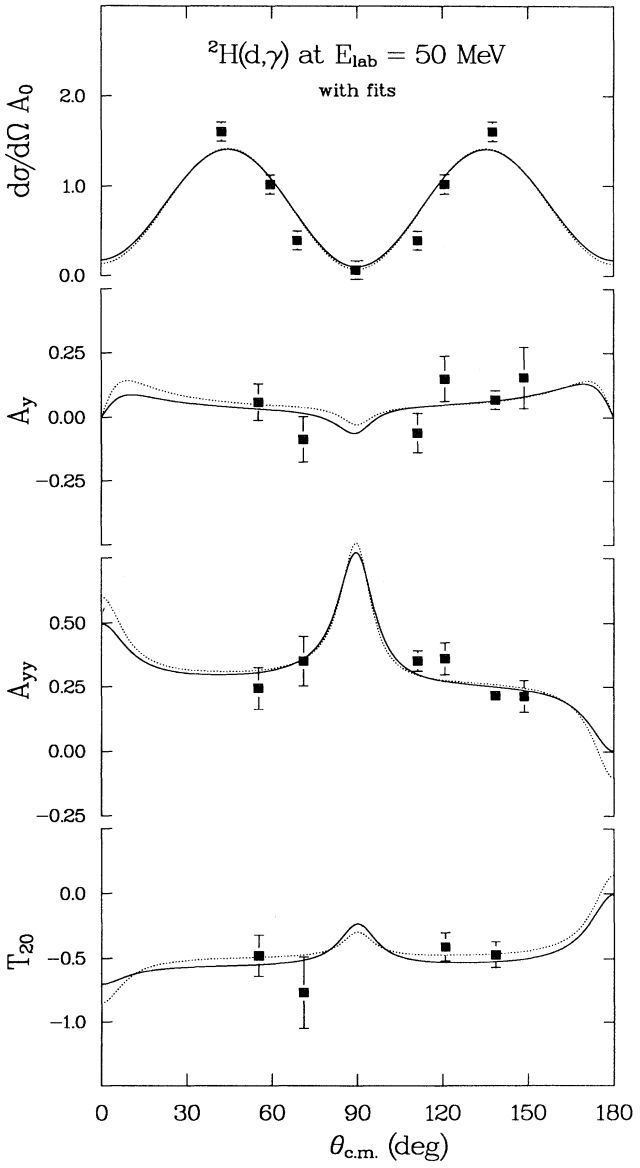

FIG. 5. 50 MeV data and TME fits. The solid curves are the result of the five-amplitude fit dicussed in the text. The dotted curves were obtained when two of these, the $^5s_5(E2)$ and the $^5d_5(E2)$, were set equal to zero.

$A_{yy}(\theta)$ is related to a combination of the C_k and E_k coefficients.

Following Ref. [21], the A_k, B_k, C_k, and E_k coefficients can be written in terms of the complex transition-matrix elements (TME's) participating in the reaction. These complex numbers (amplitudes and phases) can then be searched on to fit all of the data at a given energy. In the present work, we began with the most complete data set (E_d = 50 MeV) and included the following transition matrix elements: $^1d_5(E2)$, $^5s_5(E2)$, $^5d_5(E2)$, $^5g_5(E2)$, and $^3p_1(E1)$. Since only relative phases can be determined, the phase of the $^1d_5(E2)$ term was set equal to zero. A simultaneous search on the five amplitudes and four remaining phases was performed to fit the $\sigma(\theta)$, $A_y(\theta)$, $A_{yy}(\theta)$, and $T_{20}(\theta)$ data. The results of this procedure are shown along with the data in Fig. 5 and tabulated in Table I. Since the $^5s_5$ and the $^5d_5(E2)$ terms were very small, they were omitted in a second fit, the results of which are also shown in Fig. 5 and Table I. These results indicate that 14±8% of the cross section at 50 MeV is due to g-wave capture from the $S = 2$ $l = 4$ continuum state. The remaining strength is due to d-wave capture from the $S = 0$ $l = 2$ continuum state. The g-wave strength predicted by the direct capture model described below is 9%, and, within the rather large uncertainty, agrees with the experimental value.

The results of this fit at 50 MeV were taken as starting values for the 30 MeV data. The results of the search at 30 MeV produced the fits shown in Fig. 6 and tabulated in Table I. Once again, the cross section is dominated by d-wave $E2$ capture having $S = 0$. The g-wave – $S = 2$ – $E2$ capture strength comprises 7.0 ± 4.5% of the cross section, while the total $S = 2$ $E2$ capture strength accounts for 13.3% of the cross section at 30 MeV. The data at 20 MeV, shown in Fig. 8, were inadequate for this type of analysis.

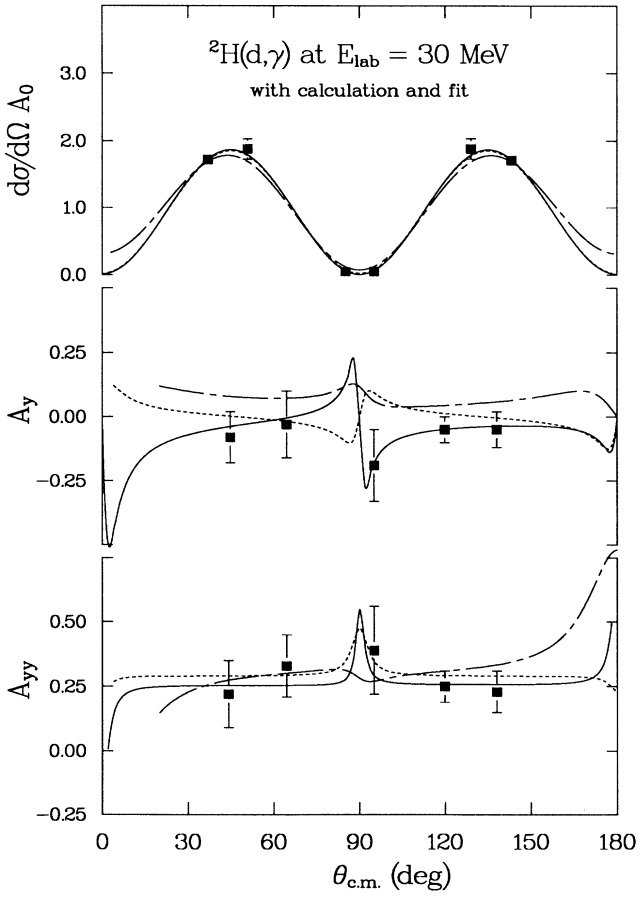

FIG. 6. 30 MeV data, calculations, and TME fits. The solid curve is the fit, the dashed curve is the direct capture calculation, and the chain-dashed curve is the RGM calculation.

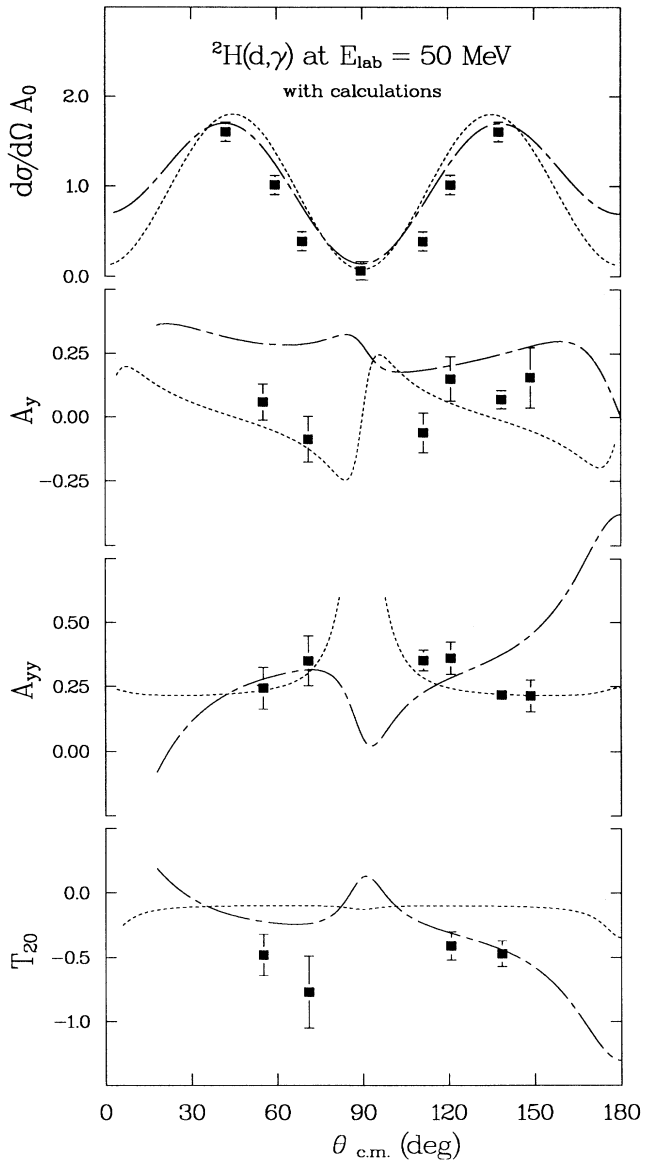

FIG. 7. 50 MeV data and calculations. The dashed curve is the direct capture calculation and the chain-dashed curve is the RGM calculation.

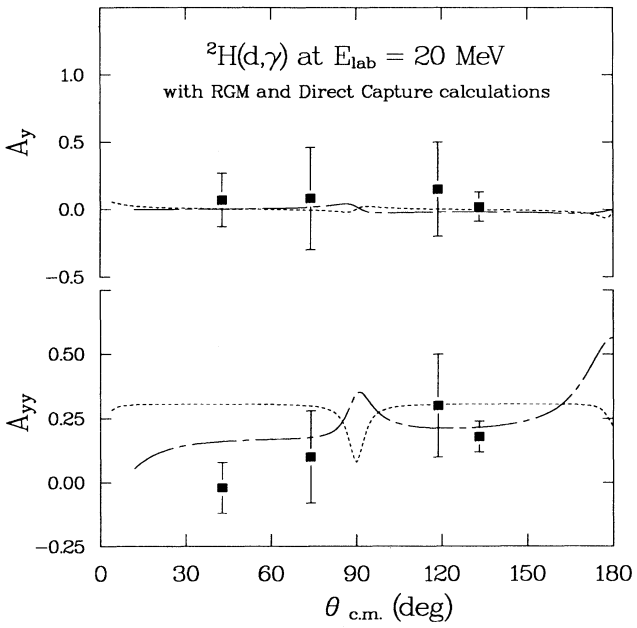

FIG. 8. 20 MeV data and direct capture (dashed curve) and RGM calculations (chain-dashed curve).

IV. DIRECT CAPTURE CALCULATION

A direct capture calculation was performed under the assumption of a pure $E2$ transition. In this calculation, observables were computed from matrix elements of the form $\langle u \mid r^2 \mid \Psi \rangle$, where u is the bound state wave function, Ψ is the continuum wave function, and r^2 is the $E2$ operator in the long wavelength limit. These wave functions were constructed from potentials: the bound state potentials were Woods-Saxon wells whose depths were obtained for the S- and D-wave two-point-deuteron components of the ground state of ^{4}He by varying them to reproduce the binding energy of ^{4}He. The continuum potential was produced by an optical model fit to the ^{2}H$(d,d)^2$H elastic scattering data at 30 MeV [22] and 50 MeV [23]. Various optical potentials could be found which fit the elastic scattering data for different values of V and its radius parameter r_0 due to the Vr_0^n ambiguity. It was found that especially small values of r_0 ($r_0 = 1.3$ fm) produced poor agreement with the T_{20} data. In fact, T_{20} had the wrong sign at 50 MeV [$T_{20}(130°) = 0.55$]. This calculation predicted a capture cross section which contained about 2% g-wave capture to the D state of ^{4}He. Increasing the radius of the real well (r_0) while searching on V to maintain a good fit to the elastic scat-

TABLE I. TME's,[a] from fits, direct capture, and MCCRGM calculations at 30 and 50 MeV.

50 MeV amplitudes	From fits	(No s or d to D)	MCC	Direct capture
$^1d_5(E2)$	0.74 +/− 0.39	0.86 +/− 0.07	0.566	0.888
$^5d_5(E2)$	0.02 +/− 0.07		0.179	0.017
$^5g_5(E2)$	0.24 +/− 0.30	0.14 +/− 0.08		0.088
$^5s_5(E2)$	0.004 +/− 0.010		0.035	0.007
$^3p_1(E1)$	0.006 +/− 0.006	0.01 +/− 0.01	0.107	
$^3p_2(M2)$			0.079	
$^5d_1(M1)$			0.033	
Phases relative to the $^1d_5$ amplitude (deg)				
$^5d_5(E2)$	100 +/− 61		30	−1.0
$^5g_5(E2)$	233 +/− 65	214 +/− 32		289
$^5s_5(E2)$	indeterminate		320	222
$^3p_1(E1)$	87 +/− 74	62 +/− 60 40		
$^3p_2(M2)$	-		285	
$^5d_1(M1)$			355	
30 MeV amplitudes				
$^1d_5(E2)$	0.86 +/− 0.23		0.807	0.967
$^5d_5(E2)$	0.037 +/− 0.015		0.129	0.020
$^5g_5(E2)$	0.07 +/− 0.045			0.008
$^5s_5(E2)$	0.026 +/− 0.030		0.021	0.005
$^3p_1(E1)$	0.003 +/− 0.005		0.019	-
$^3p_2(M2)$			0.012	
$^5d_1(M1)$			0.012	
Phases relative to the $^1d_5$ amplitude (deg)				
$^5d_5(E2)$	59 +/− 8		30	0
$^5g_5(E2)$	255 +/− 8			283
$^5s_5(E2)$	233 +/− 22		300	242
$^3p_1(E1)$	278 +/− 96		25	
$^3p_2(M2)$			275	
$^5d_1(M1)$			350	

[a]Amplitudes are presented as the percentage contribution to the cross section.

TABLE II. Parameters for direct capture calculation.

Optical model potential well parameters	
V	70.63 MeV
r_0	1.6 fm
a	0.592 fm
W_s	2.7 MeV
r_w	1.6 fm
a_w	0.75 fm
Bound state well parameters	
V_s	61.37 MeV
r_s	1.6 fm
a_s	0.5
V_D	162.74
r_D	1.6 fm
a_D	0.5

tering data produced potentials which led to more g-wave capture and gave realistic negative values of $T_{20}(130°)$. For example, $r_0 = 2.1$ gave $T_{20}(130°) = -0.64$ with an $A_{yy} = 0.13$. This result predicted a cross section which consisted of 95% g-wave capture strength, suggesting that the negative value of T_{20} arises from the presence of g-wave capture. This large g-wave admixture, however, produced an angular distribution of the cross section with a very large yield at 90° [$\sigma(90°) = \sigma(135°)$], unlike the data. It was found that the choice of $r_0 = 1.6$ fm produced a solution which contained 9% g-wave capture and gave the best overall result. The optical model potential parameters found for $r_0 = 1.6$ fm were $V = 70.63$ MeV, $a = 0.592$ fm, $W_s = 2.7$ MeV, $r_w = 1.6$ fm and $a_w = 0.75$ fm. The bound state parameters were $V_s = 61.37$ MeV, $r_s = 1.6$ fm, $a_s = 0.5$, $V_D = 162.74$, $r_D = 1.6$ fm, and $a_D = 0.5$. These parameters are summarized in Table II. The value of A_{yy} predicted by this calculation is proportional to the amount of D state included in the ground state of ^{4}He. This value was varied and it was found that a 4% admixture best fit the data at 20, 30, and 50 MeV, which agrees with the result of a similar analysis performed at E_d(lab) = 10 MeV [5]. Although this result appears to be a smaller number than predicted by most of the theories [1], it must be remembered that this is only the $l = 2$ probability when the ^{4}He nucleus is in a two-point-deuteron configuration and is not the entire D state. This number can be compared to the 2.2% result of Ref. [24].

TABLE III. TME's from direct capture and MCCRGM calculation at 20 MeV.

20 MeV amplitudes	MCCRGM	Direct capture
$^1d_5(E2)$	0.8076	0.975
$^5d_5(E2)$	0.1402	0.020
$^5g_5(E2)$		0.001
$^5s_5(E2)$	0.0224	0.004
$^3p_1(E1)$	0.0135	
$^3p_2(M2)$	0.0088	
$^5d_1(M1)$	0.0076	
Phases relative the $^1d_5$ amplitude (deg)		
$^5d_5(E2)$	30	0
$^5g_5(E2)$		292
$^5s_5(E2)$	290	269
$^3p_1(E1)$	10	
$^3p_2(M2)$	260	
$^5d_1(M1)$	0	

The results of this direct capture calculation, presented in Figs. 6–8, and Tables I and III, give a fairly good description of all of the data at 20, 30, and 50 MeV, with the exception of T_{20} and $d\sigma/d\Omega$ at 50 MeV. One probable reason for this failure was previously discussed: the deuteron D-state effects. An additional explanation of this failure could be the fact that the s-wave scattering state is highly distorted and therefore difficult to describe with this model [25].

V. THE MICROSCOPIC COUPLED-CHANNEL RESONATING GROUP MODEL

The most recently published theoretical work on the the ^{2}H(d,γ)^{4}He reaction is a microscopic coupled-channel resonating group model (MCCRGM) calculation [24]. This work treats the incoming channel in a much more sophisticated way but still suffers from the use of only a semirealistic nucleon-nucleon force and does not include D states in the fragments. In this publication the authors show good agreement with the 10 MeV data [8], and later publications [6,26] showed that the calculation worked well at 1.2 MeV as well. This calculation can also be compared to the present data at energies up to 50 MeV. There is qualitative agreement in this region, despite the fact that the $\langle ^5D_0|E2|^5g_2\rangle$ amplitude is expected to contribute significantly in this energy region [27], as seen in the TME analysis above. The MCCRGM calculation includes the ^{3}H-p and ^{3}He-n channels in addition to the d-d channel. The two-body force used here is a so-called "semirealistic" nucleon-nucleon force derived in earlier work by the same group [28] and contains Coulomb, central, spin-orbit, and tensor components. Angular momenta up to $l = 2$ were included in the relative motion of the fragments in the scattering state. No internal angular momentum (D state) was included in any of the fragments. The ground state of ^{4}He was made up of these fragments as well as a linear combination of $\langle ^1S_0 \mid (^3$H-$p)$, $\langle ^1S_0 \mid (^3$He-$n)$, $\langle ^1S_0 \mid (d$-$d)$, and $\langle ^5D_0 \mid (d$-$d)$ components, in the most tightly bound 0^+ configuration. Calculation of the $E2$ strength included the seven coupled channels: $\langle ^1S_0|(^3$H-$p)|E2|^1d_2\rangle$, $\langle ^1S_0|(^3$H-$p)|E2|^3d_2\rangle$, $\langle ^1S_0|(^3$He-$n)|E2|^1d_2\rangle$, $\langle ^1S_0|(^3$He-$n)|E2|^3d_2\rangle$, $\langle ^1S_0|(d$-$d)|E2|^1d_2\rangle$, $\langle ^1S_0|(d$-$d)|E2|^5d_2\rangle$, and $\langle ^5D_0|(d$-$d)|E2|^5s_2\rangle$. $E1$, $M1$, and $M2$ transitions were also included. Notably lacking is the $\langle ^1S_0 \mid (d$-$d) \mid E2 \mid ^5 s_2\rangle$ transition strength which involves an internal D state of the deuteron. This amplitude is expected to be especially important at low energy. Also note that the $\langle ^5D_0 \mid (d$-$d) \mid E2 \mid ^5 g_2\rangle$ amplitude is not included. As previously shown, TME fits and direct capture calculations indicate that the g waves contribute at about the 10% level at 50 MeV. The matrix elements were calculated over the range of energies from a few keV up to 50 MeV, but the authors [24] only compared their results to the astrophysical S factor as a function

of energy and to the data set at 10 MeV. Besides the fact that the most complete data set exists at 10 MeV, this is probably also the energy where this calculation is most appropriate in light of the deficiencies at higher and lower energies mentioned above. The observables are compared to this calculation at $E_d = 1.2$ MeV in Ref. [6], and reasonable agreement is seen.

The MCCRGM calculation has been previously shown to be in qualitative agreement with the A_{yy} data as a function of energy at $\theta = 130°$ from threshold up to 50 MeV [29]. The results of these same calculations are shown in Figs. 6, 7, and 8, along with the present data and the direct capture model calculation. The resulting TME's are presented in Tables I and III. While the coupled channels resonating group model with the p-^{3}H and n-^{3}He channels included exhibits rather good agreement with the experimental results over the entire energy range up to 50 MeV, some deficiencies are also apparent.

While shedding some light on this reaction, this calculation has raised many questions and clearly should be improved. Use of a more realistic nucleon-nucleon force, inclusion of the deuteron D state, and inclusion of higher partial waves (g waves), would help to clarify the situation. It should be pointed out that this MCCRGM calculation was performed before our data existed (or any in this energy region). The authors of this calculation have stated [30] that the calculation is presently being redone with a more realistic N-N force and including D-state components in all fragments.

VI. CONCLUSIONS

The qualitative aspects of this work as well as the lower energy work on this reaction are remarkably well explained by the calculations of Hofmann [24] which predict a 2.2% $d+d$ D-state probability in the ground state of ^{4}He. While there is general agreement, there are important specific discrepancies which require further theoretical study. A calculation which uses a realistic two-body force which includes D states in the fragments (especially the deuteron) and which includes g-wave capture (at the higher energies) is needed. In order to facilitate the comparison of future calculations with the data of this work, the present data are presented in Table IV. The present direct capture calculations, while extremely simple, give a good description of most of the data between 20 and 50 MeV. This calculation implies a $d+d$ D-state component in the ground state of ^{4}He of 4%. Both these calculations and the T-matrix element analysis at 50 MeV indicate that the D state of ^{4}He is playing a significant role in determining the cross section for this reaction at these energies: At 50 MeV about 15% of the $E2$ strength arises from capture to the D state. The TME analysis and the direct capture model also agree on the fact that g-wave ($E2$) capture is significant in the

TABLE IV. Tabulated values of the measured observables.

c.m. angle (deg)	$d\sigma/d\omega A_0$	$\Delta d\sigma/d\omega A_0$	A_y	ΔA_y	A_{yy}	ΔA_{yy}	T_{20}	ΔT_{20}
50 MeV								
42.2	1.60	0.10						
55.2			0.06	0.07	0.24	0.08	-0.48	0.16
59.5	1.01	0.10						
69.0	0.39	0.10						
71.1			-0.087	0.090	0.351	0.097	-0.77	0.28
89.6	0.06	0.10						
90.6	0.06	0.10						
111.3	0.39	0.10	-0.06	0.07	0.35	0.04		
120.8	1.01	0.10	0.150	0.087	0.361	0.063	-0.41	0.11
137.6	1.60	0.1	0.069	0.036	0.217	0.024	-0.47	0.10
148.6			0.15	0.12	0.21	0.06		
30 MeV								
37.0	1.72	0.09						
44.4			-0.08	0.10	0.22	0.13		
50.8	1.88	0.15						
64.5			-0.03	0.13	0.33	0.12		
85.0	0.049	0.026						
95.1	0.050	0.027	-0.19	0.14	0.39	0.17		
119.8			-0.05	0.05	0.25	0.06		
129.1	1.88	0.15						
138.0			-0.05	0.07	0.23	0.08		
143.2	1.71	0.09						
20 MeV								
42.8			-0.07	0.20	-0.02	0.10		
74.0			-0.08	0.38	0.10	0.18		
118.7			-0.15	0.35	0.30	0.20		
133.1			0.02	0.11	0.18	0.06		

50 MeV region. We have also seen that non-$E2$ radiation is relatively insignificant at these energies. Clearly, future experimental work should be directed at obtaining precision data on all polarization observables. Such data should allow for precise determination of all $E2$, $E1$, and $M2$ transition-matrix elements. A comparison of these with model predictions should provide further insight into both the reaction theory and the detailed role of the D state of ^{4}He in this reaction.

ACKNOWLEDGMENTS

The authors wish to thank the managements of the Kernfysisch Versneller Institute and the Lawrence Berkeley Laboratory for their hospitality, and the staffs at both institutions for very essential help. This work was partially supported by the U.S. Department of Energy, Office of High Energy and Nuclear Physics, under Grant No. DEFG05-91-ER40619.

[1] H.R. Weller and D.R. Lehman, Annu. Rev. Nucl. Part. Sci. **38**, 563 (1988).
[2] P. Goldhammer, Phys. Rev. C **29**, 1444 (1984).
[3] M.R. Meder, P. Chiang, and J.L. Purcell, Bull. Am. Phys. Soc. **33**, 929 (1988).
[4] J. Carlson, Phys. Rev. C **38**, 1879 (1988).
[5] H.R. Weller *et al.*, Phys. Rev. C **34**, 32 (1986).
[6] J.L. Langenbrunner *et al.*, Phys. Rev. C **38**, 565 (1988).
[7] S. Mellema, T.R. Wang, and W. Haeberli, Bull. Am. Phys. Soc. **30**, 1268 (1985); **32**, 1547 (1987).
[8] S. Mellema, T.R. Wang, and W. Haeberli, Phys. Lett. **166B**, 282 (1986).
[9] S. Mellema, T.R. Wang, and W. Haeberli, Phys. Rev. C **34**, 2043 (1986).
[10] P. Corvisiero *et al.*, Few-Body Syst. **10**, 135 (1991).
[11] W.K. Pitts *et al.*, Phys. Rev. C **37**, 1 (1988); Ph.D. dissertation, Indiana University (1987).
[12] H. Flowers and F. Mandl, Proc. R. Soc. London A **206**, 131 (1950).
[13] E.K. Warburton and J. Weneser, in *Isospin in Nuclear Physics*, edited by D.K. Wilkinson (North-Holland, Amsterdam, 1969), Vol. 185.
[14] S. deBenedetti, *Nuclear Interactions* (Wiley, New York, 1964).
[15] H.R. Weller, J. Phys. Soc. Jpn. **55**, 113 (1986); Comments Nucl. Part. Phys. **17**, 25 (1987).
[16] D.R. Lehman and H.R. Weller (unpublished).
[17] F.S. Dietrich and D.W. Heikkinen, Nucl. Instrum. Methods **155**, 103 (1978).
[18] H.F. Glavish, in *Proceedings of the Third Polarization Symposium*, edited by H. Barschall and W. Haeberli (University of Wisconsin Press, Madison, 1970).
[19] D.J. Clark *et al.*, in *Procceedings of the Fifth Cyclotron Conference*, edited by R. W. McIlroy (Butterworths, London, 1971), Vol. 610.
[20] P.R. Bevington, *Data Reduction and Error Analysis for the Physical Sciences* (McGraw-Hill, New York, 1963), Vol. 290.
[21] R.G. Seyler and H.R. Weller, Phys. Rev. C **20**, 453 (1979).
[22] Nemets *et al.*, Ukr. Fiz. Zh. (Russ. Ed.) **30**, 328 (1985).
[23] C. Alderliesten *et al.*, Phys. Rev. C **18**, 2001 (1978).
[24] B. Wachter, T. Mertelmeier, and H. M. Hofmann, Phys. Lett. B **200**, 246 (1988).
[25] J.A. Tostevin, Phys. Rev. C **34**, 1497 (1986).
[26] J.L. Langenbrunner *et al.*, Phys. Rev. C **42**, 1214 (1990).
[27] Anna Eiro (private communication).
[28] T. Mertelmeier and H.M. Hofmann, Nucl. Phys. **A459**, 387 (1986).
[29] H.R. Weller *et al.*, Phys. Lett. B **213**, 413 (1988).
[30] H.M. Hofmann (private communication).